International Journal of Refrigeration 136 (2022) 8–16

Contents lists available at ScienceDirect

International Journal of Refrigeration

journal homepage: www.elsevier.com/locate/ijrefrig

Experimental assessment of different extraction points for the integrated mechanical subcooling system of a CO_2 transcritical plant

Évaluation expérimentale de différents points d'extraction pour le systéme de sous-refroidissement mécanique intégré d'une installation au CO_2 transcritique

Laura Nebot-Andrés *, Daniel Calleja-Anta, Carlos Fossi, Daniel Sánchez, Ramón Cabello, Rodrigo Llopis

Thermal Engineering Group, Mechanical Engineering and Construction Department, Jaume I University, Spain

ARTICLE INFO

Keywords:
Experimental comparative
Subcooling
Integrated mechanical subcooling
Transcritical CO_2

Mots clés:
Comparaison expérimentale
Sous-refroidissement
Sous refroidissement mécanique intégré
CO_2 transcritique

ABSTRACT

Subcooling systems are positioned in recent years as one of the best solutions to improve the efficiency of transcritical CO_2 cycles. Specifically, the integrated mechanical subcooling cycle allows the improvement of these systems only using CO_2 as a refrigerant. This integrated cycle can be designed with three different architectures: extracting the CO_2 from the gas-cooler outlet, from the subcooler outlet or from the liquid tank. In this work, the three configurations are experimentally analysed and the main differences between them are studied. An experimental plant has been tested at three heat rejection levels (25.0, 30.4 and 35.1 °C) and a fixed temperature of the secondary fluid at the evaporator inlet of 3.8 °C. The results show that from an energy efficiency point of view, all the configurations have practically the same COP, with certain variations in the cooling capacity and the greatest differences in the cycles are found in the subcooler.

1. Introduction

Carbon dioxide has been positioned as one of the only refrigerants that can be used in centralized commercial refrigeration, due to the restrictions imposed by F-gas (European Commission, 2014). The use of CO_2 allows direct emissions to be reduced, but its low performance at high temperatures makes indirect emissions an added problem. That is why the refrigeration sector seeks to develop technologies that improve the efficiency of classic CO_2 systems (Gullo et al., 2018; Karampour and Sawalha, 2018). These solutions go through the design of more complex plants where systems such as the parallel compressor (Nebot-Andrés et al., 2021a; Sarkar and Agrawal, 2010) or the ejector (Gullo et al., 2019; Lawrence and Elbel, 2019) are used to improve the COP of the facilities. Mechanical subcooling methods have become one of the most popular strategies in recent years for the improvement of CO_2 refrigeration cycles (Llopis et al., 2018). After the use of the internal heat exchanger (IHX) as a way of improvement of cooling capacity and COP in CO_2 transcritical cycles (Rigola et al., 2010), the use of the dedicated mechanical subcooling (DMS) became popular as a method to improve the COP and the cooling capacity of said system (Catalán-Gil et al., 2019; Cortella et al., 2021; Nebot-Andrés et al., 2021b). The DMS bases its operation on the use of an auxiliary cycle, thermally coupled to the main cycle through a heat exchanger, called subcooler. This cycle, thanks to the subcooling that it produces in the CO_2 at the outlet of the gas-cooler, manages to reduce the optimum working pressure as well as increase the specific cooling capacity (Llopis et al., 2015). On the contrary, this cycle works with a refrigerant other than CO_2. The DMS was first tested experimentally by Llopis et al. (2016) reaching increments up to 30.3% on COP compared to the base cycle even though the degree of subcooling was not optimized. Later, its optimum operation parameters were determined by Nebot-Andrés et al. (2021b).

With the aim of working with purely CO_2 cycles, the concept of integrated mechanical subcooling (IMS) was born, where the subcooling of the CO_2 at the outlet of the gas-cooler is carried out with a flow of CO_2 extracted from the main stream and evaporated through the subcooler. The most studied configuration performs this extraction from the gas-cooler exit (Nebot-Andrés et al., 2019), passing through an expansion valve and carrying out the evaporation process inside the subcooler, to be recompressed by the secondary compressor and reintroduced into the

* Corresponding author.
E-mail address: lnebot@uji.es (L. Nebot-Andrés).

https://doi.org/10.1016/j.ijrefrig.2022.01.006
Received 21 September 2021; Received in revised form 3 January 2022; Accepted 4 January 2022
Available online 6 January 2022

Nomenclature

COP	coefficient of performance
Cp	specific heat capacity, kJ•kg^{-1}• K^{-1}
GCO	extraction from gas-cooler outlet configuration
$\dot{m}$	mass flow, kg•s^{-1}
p	absolute pressure, bar
Pc	power consumption, kW
$\dot{Q}$	cooling capacity, kW
SUB	degree of subcooling produced in the subcooler, K
SCO	extraction from subcooler outlet configuration
t	temperature, °C
TNK	extraction from liquid tank configuration

Greek symbols

ε	uncertainty
ρ	density, kg•m−3
f	frequency, Hz
τ	compression ratio

Subscripts

gly	propylene glycol–water mixture
gc	gas-cooler
IMS	corresponding to the IMS cycle
in	inlet
main	corresponding to the main cycle
0	evaporating level
o	outlet
ps	pseudocritical
sub	corresponding to the subcooler
suc	compressor suction
tkn	corresponding to the liquid tank
w	water

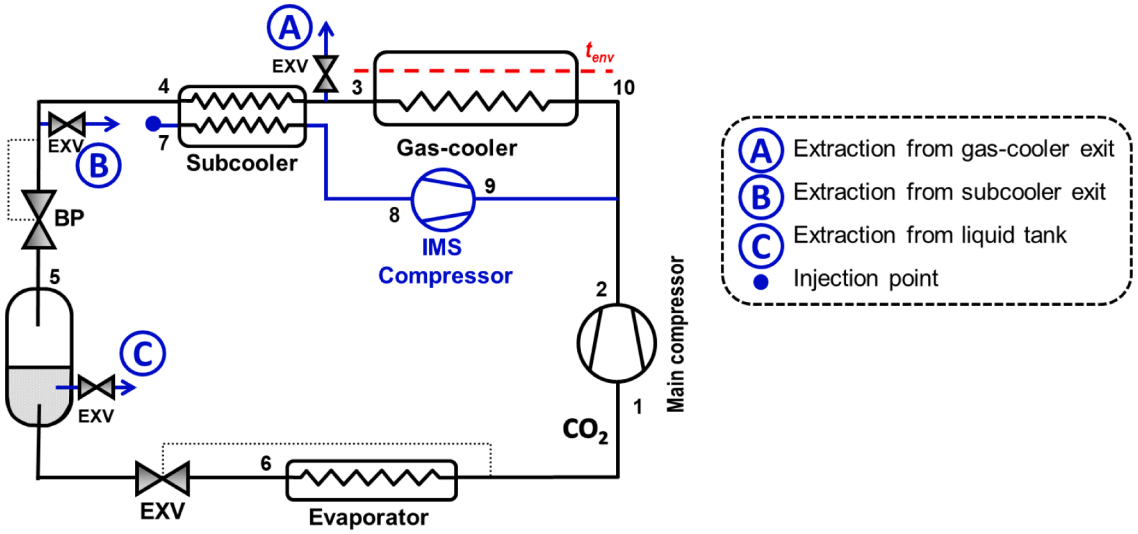

Fig. 1. Configuration plant.

main stream. The advantage of this configuration is that only the CO_2 flow that is going to reach the evaporator is subcooled, therefore a smaller subcooler is necessary. However, it is also possible to carry out this cycle in two other configurations: extracting from the tank's liquid exit or extracting from the subcooler outlet.

As all subcooling methods working on transcritical CO_2 plants, two operating parameters must be optimized. They are the gas-cooler pressure and also the subcooling degree. The experimental determination of the optimum working conditions of the integrated mechanical subcooling was first determined by Nebot-Andrés et al. (2020). The evaluated configuration was the one with the extraction from the subcooler exit. The optimum COP values were also determined in this work. Although this configuration was analysed, the other two have never been experimentally tested and therefore it has not been possible to determine which of them is better.

The objective of this work is to experimentally compare the three possible configurations of the IMS and determine which of them is more convenient for its application. For this, the three configurations have been tested for three different heat rejection levels ($t_{w,in}$ = 25.0, 30.4 and 35.1 °C) and one cold level ($t_{gly,in}$ = 3.8 °C) in a single compression refrigeration plant with a two-stage expansion system.

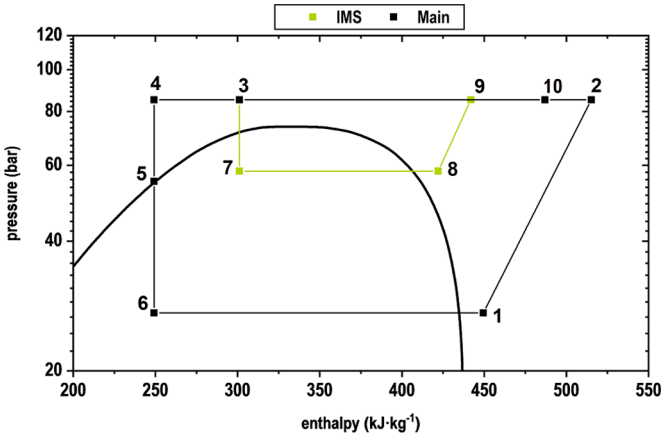

Fig. 2. pH Diagram of GCO configuration ($t_{w,in}$ = 30.4 °C).

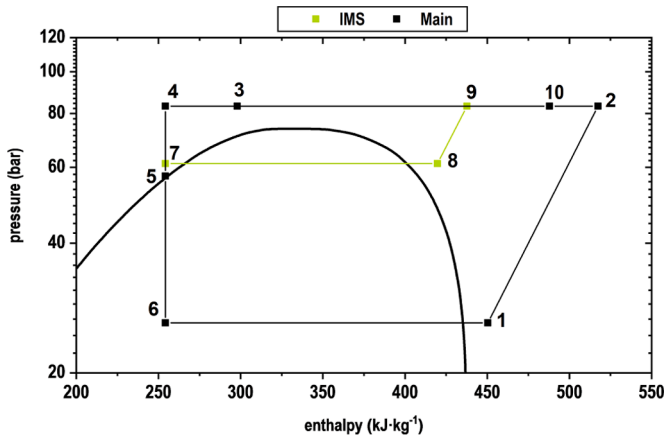

Fig. 3. pH Diagram of SCO configuration ($t_{w,in}$ = 30.4 °C).

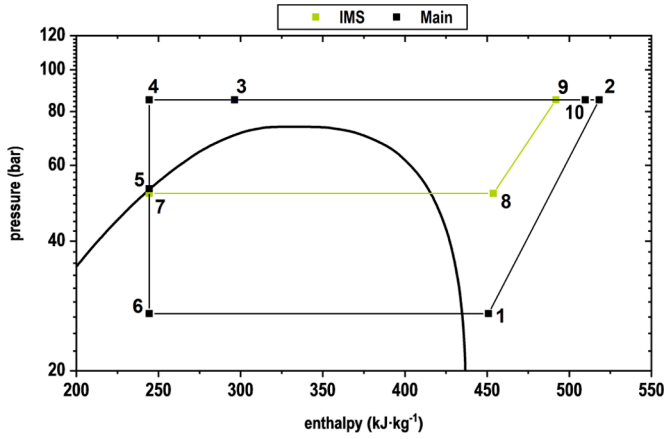

Fig. 4. pH Diagram of TNK configuration ($t_{w,in}$ = 30.4 °C).

2. Integrated mechanical subcooling configurations and experimental procedure

In this section, the three possible configurations of the Integrated Mechanical Subcooling system are presented and described. Also the description of the experimental plant is included and the test procedure is explained.

2.1. Cycle configurations

The three configurations of the IMS are presented in Fig. 1. The cycle with extraction from the gas-cooler outlet (GCO) is represented as point A in Fig. 1 and the pH diagram in Fig. 2, the extraction from the exit of the subcooler as point B in Fig. 1 (SCO) and Fig. 3 and from the liquid tank (TNK) as point C in Fig. 1 and Fig. 4.

As it can be seen, the main difference amongst the cycles is the extraction point. The rest of the cycle, marked in blue, is similar. An electronic expansion valve produces the expansion of the extracted mass flow and its evaporation is performed in the subcooler, to later be recompressed through the IMS compressor and reinjected in the discharge line.

The different extraction points have a direct effect on the heat exchanged in the subcooler. Said exchange is calculated as shown in Eq. (1): it is the product of the mass flow transferred by the IMS compressor and the enthalpy difference between the inlet and outlet of the subcooler.

$$\dot{Q}_{sub} = \dot{m}_{IMS} \cdot (h_8 - h_7) \tag{1}$$

$$h_8 = f(T_8, p_8) \tag{2}$$

$$h_7 = h_{gc,o} = f(T_3, p_3) \textbf{forGCOconfiguration} \tag{3}$$

$$h_7 = h_{sub,o} = f(T_4, p_4) \textbf{forSCOconfiguration} \tag{4}$$

$$h_7 = h_{tnk,o} = f(P_5, x = 0) \textbf{forTNKconfiguration} \tag{5}$$

The outlet enthalpy (h_8) is calculated in the same way for all three configurations: from the temperature and pressure at the outlet of the subcooler, as shown in Eq. (2), although its value will depend on the degree of subcooling and the working pressure. On the other hand, the input enthalpy depends on the extraction point, which is different in every case.

For the GCO configuration, considering isenthalpic expansion, the inlet enthalpy is equal to the enthalpy at the exit of the gas-cooler; Eq. (3), for the SCO configuration, the inlet enthalpy is equal to the enthalpy at the exit of the subcooler, Eq.(4) and for the TNK configuration, the inlet enthalpy is equal to the enthalpy at the exit of the vessel, saturated-liquid, Eq.(5).

Neither the enthalpy difference is the same for the three configurations nor the flow transferred by the compressor, since it will depend on the rotation speed. Therefore, the behaviour of each configuration will depend on the heat exchanged in the subcooler and at the same time in the part of the flow diverted by the IMS.

2.2. Description of the plant and measurement system

The experimental plant tested in this work is presented in Nebot-Andrés et al. (2020). The plant is a CO_2 single-stage transcritical refrigeration system with an integrated mechanical subcooling system. The plant allows testing the three configurations: extracting gas at the exit of the subcooler (SCO), from the exit of the gas-cooler (GCO) and from the liquid tank (TNK). The main single-stage refrigeration cycle uses a semi-hermetic compressor with a displacement of 3.48 $m^3 \bullet h^{-1}$ at 1450 rpm and a nominal power of 4 kW. The expansion is carried out by a double-stage system, composed of an electronic expansion valve (back-pressure) controlling the gas-cooler pressure, a liquid receiver between stages and an electronic expansion valve, working as thermo-static, to control the evaporating process. Evaporator and gas-cooler are brazed plate counter-current heat exchangers with exchange surface area of 4.794 m^2 and 1.224 m^2, respectively. The subcooler is situated directly downstream of the gas-cooler. It is a brazed plate heat exchanger with an exchange surface area of 0.850 m^2. It works as the evaporator of the mechanical subcooling system for all configurations and subcools the CO_2 at the exit of the gas-cooler. The IMS cycle is driven by a variable speed semihermetic compressor with displacement of 1.12 $m^3 \bullet h^{-1}$ at 1450 rpm. The expansion valve of the IMS cycle is electronic, working as thermostatic, controlling the superheat in the evaporator of the subcooler. Heat dissipation in gas-cooler is done with a water loop, simulating the heat rejection level. The evaporator is supplied with another loop, working with a propylene glycol–water mixture (60% by volume) that enables a constant entering temperature in the evaporator. Both the mass flow and the inlet temperature are controlled in these loops.

All fluid temperatures are measured by T-type thermocouples and pressure gauges that are installed along all the circuit. CO_2 mass flow rates are measured by Coriolis mass flow meters, as well as the secondary fluids. Compressors' power consumptions are measured by two digital wattmeters. The accuracies of the measurement devices can be consulted in Nebot-Andrés et al. (2020).

2.3. Test procedure

The description of the experimental tests procedure is detailed in this section. To evaluate the refrigeration plant using the different

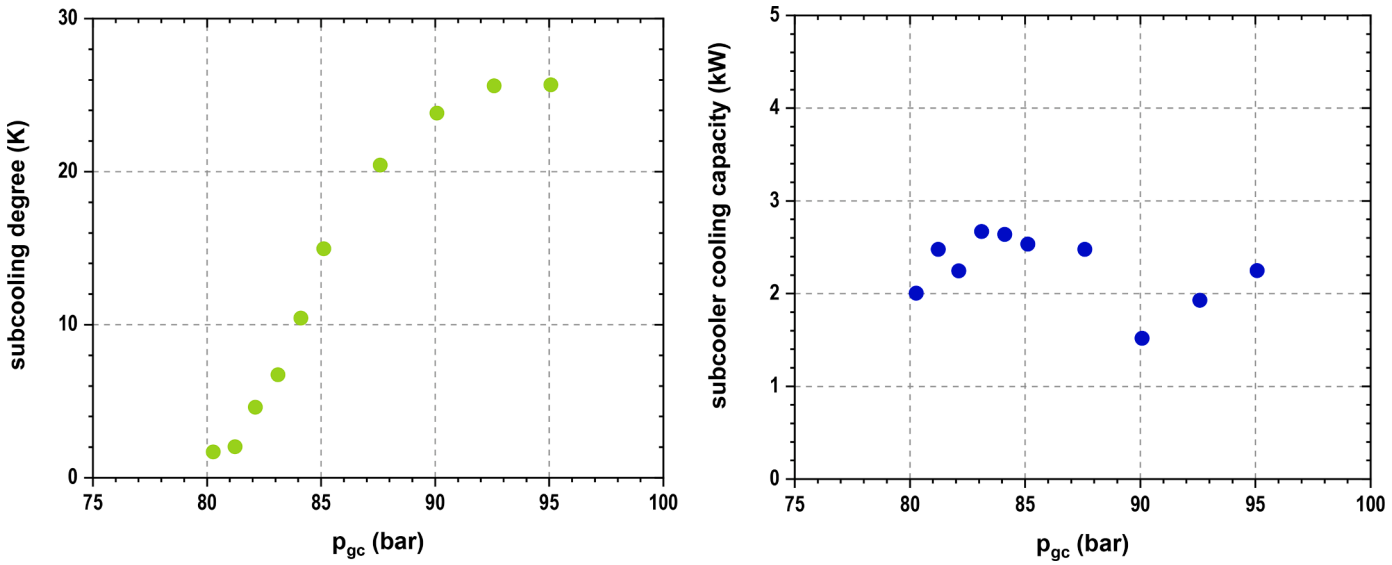

Fig. 5. Subcooling degree and subcooler cooling capacity for GCO vs gas-cooler pressure (40 Hz, $t_{w,in}$ = 30.4 °C) .

configurations of the integrated mechanical subcooling, each configuration has been tested at identical working conditions, always operating in the transcritical region. The evaluated conditions were:

- Heat rejection level: three different temperatures: 25.0, 30.4 and 35.1 °C, with maximum deviation of ±0.20 °C. These levels were performed fixing the temperature of the secondary fluid (water) at the entrance of the gas-cooler and maintaining the water flow rate to 1.17 m^3h^{-1}.
- One inlet temperature of the secondary fluid in the evaporator: 3.8 ± 0.12 °C. The flow rate was fixed to 0.7 m^3h^{-1}.
- Gas-cooler pressure was regulated with an electronic BP fixed during each test thanks to a PDI controller. For each condition, tests were performed at different pressures in order to identify the optimum one and reach the optimum COP conditions, as done in previous experiments with this plant. The optimization process can be consulted in detail in Nebot-Andrés et al. (2020).
- Compressors: The main compressor always operated at nominal speed of 1450 rpm. The speed of the IMS compressor was varied in order to obtain the optimum subcooling degree.
- Electronic expansion valves: The electronic expansion valves were set to obtain a superheating degree in the evaporator of 10 K and of 10 K on the subcooler. Useful superheating the evaporator and also in the subcooler of SCO and GCO has been ensured. However, it was not possible to ensure this in the TNK configuration because the pressure drop in the valve was too small.

All the tests were carried out in steady state conditions for periods longer than 10 min, taking data each 5 s, obtaining the test point as the average value of the whole test. The measured data were used to calculate the thermodynamic properties of the points using Refprop v.9.1. (Lemmon et al., 2013).

2.4. Physical limitations

This section presents some of the drawbacks that have been detected when testing the cycles and that deviate their behaviour from the results obtained in theoretical studies.

CO_2 can be subcooled as long as we are in the transcritical zone. If the plant works below the critical point, the CO_2 condenses inside the subcooler. In some of the tests, it has been observed that working at pressures close to the critical pressure (even if they are higher), the CO_2 partially condenses in the subcooler, and although the speed of the IMS

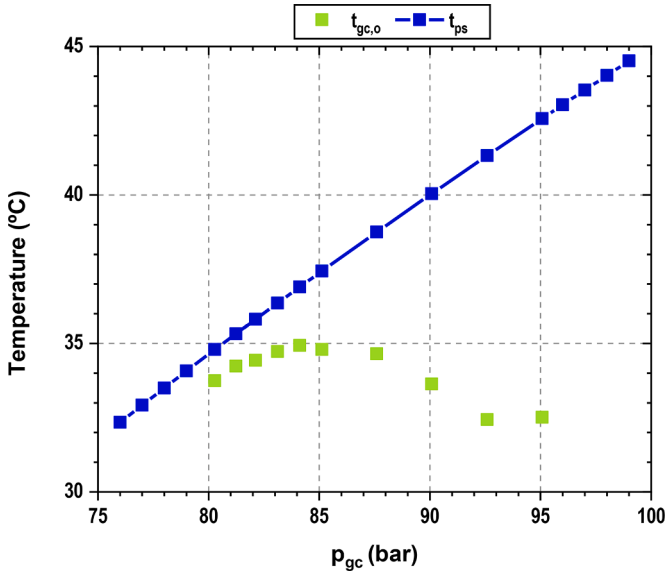

Fig. 6. Gas-cooler outlet temperature and pseudocritical temperature for GCO vs gas-cooler pressure (40 Hz, tw,in = 30.4 °C).

compressor increases, it is not possible to increase the degree of subcooling, which is around 2 K.

The cooling capacity exchanged in the subcooler, shown in Fig. 12, varies between 8% and 22% between the tests depending on the configuration when looking at optimum conditions. But going lower from a certain pressure, out of optimal conditions, depending on the test condition and the tested configuration, the subcooling does not vary significantly with the variation of the compressor speed. In these areas where subcooling cannot be carried out properly, the COP of the system goes down, therefore it is necessary to slightly increase the pressure in order to achieve the desired subcooling and with it the increase in COP.

The Fig. 5 represents the subcooling degree as a function of the pressure for a fixed rotation speed (40 Hz) for the GCO configuration. It can be seen how the subcooling degree drops significantly from 82 bar and when it reaches 93 bar it tends to a horizontal asymptote. This trend is observed in the three studied configurations. This is due to the fact that the gas-cooler outlet temperature is very close to the pseudocritical temperature, where the Cp grows drastically and therefore we are not

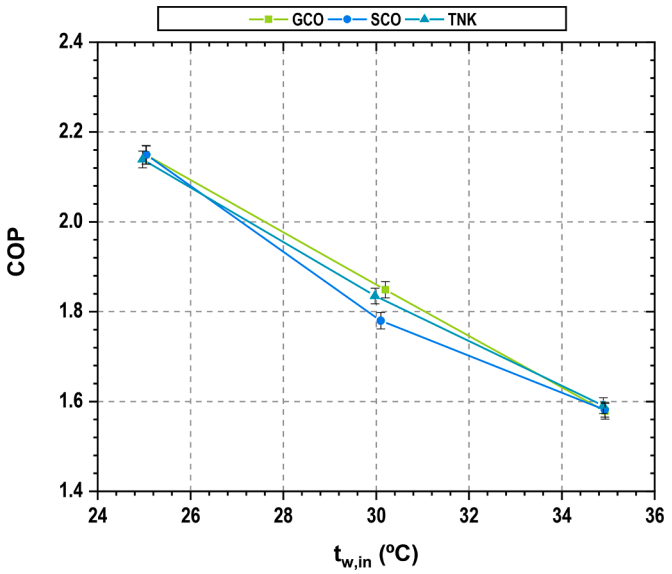

Fig. 7. Evolution of the COP of the different configurations depending on the water inlet temperature.

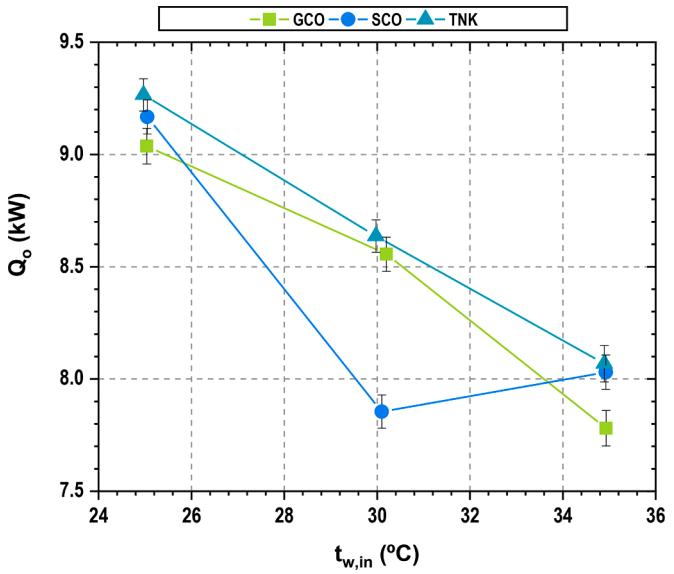

Fig. 8. Evolution of the cooling capacity of the different configurations depending on the water inlet temperature.

able to produce a large subcooling for the same cooling capacity.

The gas-cooler outlet temperature and the pseudocritical temperature (Liao and Zhao, 2002) can be observed in Fig. 6. As it can be seen, for the lowest pressures, both temperatures are very close, coinciding with the points where the achieved subcooling is low (Fig. 5). However, around 83 bar, the gas-cooler outlet temperature moves away from the pseudocritical and it is from this pressure that the trend of the subcooling degree changes. In conclusion, for the correct operation of the subcooling system, the gas-cooler outlet temperature must be far from the pseudocritical temperature. All the optimal points presented in the following section meet this condition.

As mentioned in Section 2.3, for the TNK configuration it has not been possible to ensure the superheating in the subcooler, due to the small pressure difference in the valve. In previous theoretical studies made by the authors, it has been found that the optimum point for the TNK configuration is obtained when the suction pressure of the IMS compressor is equal to the tank pressure. This cannot be achieved, as it can be seen in Fig. 4, because the expansion valve needs to be installed as security device, to avoid liquid entering the auxiliary compressor, impairing the behaviour of this configuration. This is one inconvenient of this configuration.

3. Main energy results

All the points presented in this section correspond to the optimum points (optimum subcooling degree and optimum gas-cooler pressure), identified as explained in Nebot-Andrés et al. (2020). Main results as the cooling capacity, calculated as Eq. (6), the COP, as Eq. (7), and the optimum parameters are presented in Table 2. The uncertainties are calculated using Moffat's method (Moffat, 1985) and they are also included in Table 2.

$$\dot{Q}_0 = \dot{m}_0 \cdot \left(h_{suc} - h_{sub,o}\right) \tag{6}$$

$$COP = \frac{\dot{Q}_0}{Pc_{main} + Pc_{IMS}} \tag{7}$$

3.1. Optimum COP

Fig. 7 shows the maximum COP obtained for each configuration at all the tested conditions. As it can be seen, the tendency in COP is exactly the same and the measured COP values are practically the same. It can be observed that for the water inlet conditions of 25.0 °C and 35.1 °C, the COP values can be considered identical since the differences between them are included within the measurement uncertainty. Considering the water inlet of 30 °C, slight differences can be seen in the COP, which do not exceed 2%. These differences may be due to the proximity to the pseudocritical temperature.

3.2. Cooling capacity

As it can be seen in Fig. 8, the cooling capacity decreases when the inlet temperature in the gas-cooler increases. More important differences can be seen in this parameter than in the analysis of the COP. The system that provides the greatest cooling capacity is the configuration with extraction from the tank, as can be seen in the graph. In addition, it is also important to note that this configuration provides the cooling capacity in a more constant way.

The GCO configuration provides a slightly lower cooling capacity. In addition, this configuration suffers a more abrupt drop at high temperatures. The biggest differences are found in the SCO configuration. Although for the points of 25 °C and 35 °C, the trend is very similar, for 30 °C, the cooling capacity drops significantly. This is due to its direct relationship with the degree of subcooling. The higher the subcooling is for a given condition of heat sink temperature and evaporation level, the higher the overall cooling capacity is. As will be seen later, the optimal subcooling degree for this configuration at this operating point is lower than that obtained in the other configurations. This phenomenon is due to the proximity to the pseudocritical temperature and the sensitivity of the CO_2 heat transfer parameters in this area. This phenomenon was also observed theoretically (Nebot-Andrés et al., 2019). Increasing the subcooling degree will increase the cooling capacity but will imply a reduction in COP too.

4. Optimum operation parameters

This section presents the optimal operating parameters necessary to achieve the maximum COP values.

4.1. Optimum pressure

Regarding the optimal gas-cooler pressures, for each configuration, a similar behaviour is obtained for the three configurations. It is observed

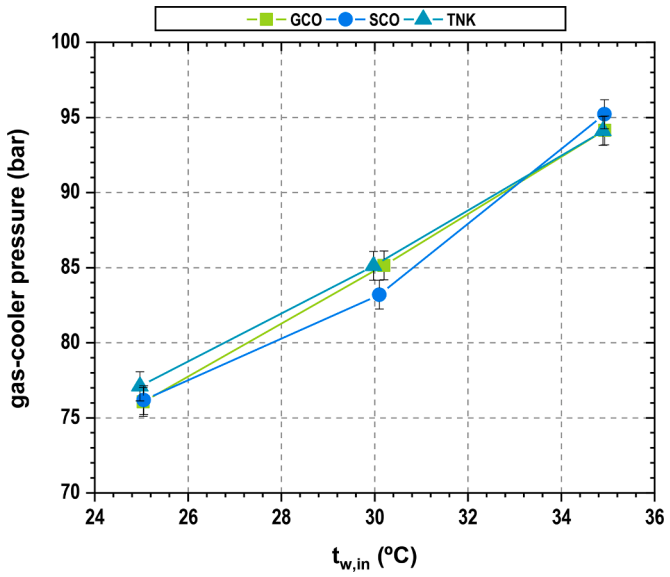

Fig. 9. Gas-cooler optimum pressures.

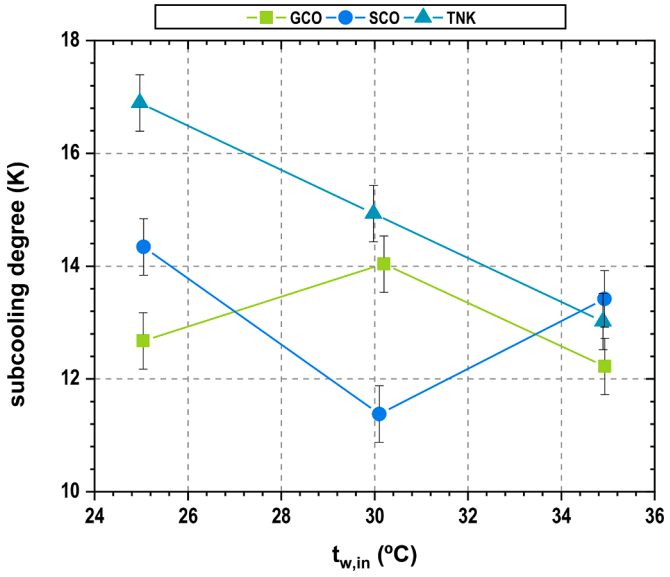

Fig. 10. Optimum subcooling degree for each configuration.

how it gets higher when the water inlet temperature to the gas-cooler increases. Optimal pressures are represented in Fig. 9. As it can be observed, optimum pressure is practically the same for the three configurations tested. A slight difference can be seen for the SCO configuration at 30 °C, but this difference is within the measurement uncertainty, so we can conclude that the optimal pressure is independent of the CO_2 extraction point. When the water inlet temperature is close to 25 °C, the optimum pressure is practically the critical pressure, while for higher temperatures, this pressure increases, until 95 bar for water inlet temperatures of 35 °C.

4.2. Optimum subcooling degree

Fig. 10 shows the optimum subcooling degree for each configuration, calculated as Eq. **Error! Reference source not found.**. As it can be seen, depending on the extraction point, the subcooling degree has a different trend. Regarding the TNK configuration, subcooling is lower when higher the water inlet temperature is. For the GCO configuration, the

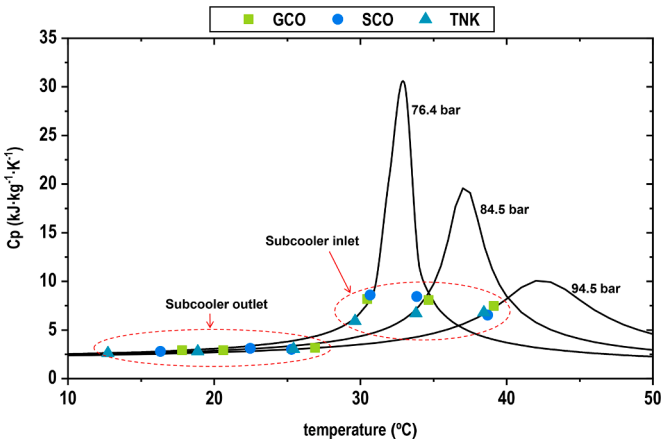

Fig. 11. Cp at inlet and outlet of the subcooler.

subcooling degree first increases and then decreases and for the SCO it follows the opposite trend.

$$SUB = t_{gc,o} - t_{sub,o} \tag{8}$$

These differences in trends are due to the gas-cooler outlet conditions, which are close to the critical point and this causes large variations in the properties of the fluid. The specific heat of the CO_2 both at the inlet and outlet of the subcooler can be seen in Fig. 11. As it can be seen, for the TNK configuration at the inlet of the subcooler, Cp has lower values compared to the other configurations and it has an growing trend with the increment of the pressure, while the other configurations have a higher Cp but its tendency is decreasing. Regarding the outlet of the subcooler, the Cp of the three configurations has the same trend, very stable, and very similar values. With this it is seen that the main differences are marked by the subcooler inlet point, which also causes differences in the optimal subcooling degree. A lower Cp, as in the case of the TNK configuration at 25.0 °C, implies higher subcooling. However, it should be mentioned that the cross of the pseudocritical region happens inside the gas-cooler for all the configurations.

Subcooling in GCO configuration first increases and then decreases. For 25.0 °C the subcooling degree is quite small because the extraction point, after the gas-cooler exit, is near the pseudocritical temperature and thus it is more difficult to perform the subcooling, as explained in Section 2.4. On the contrary, this phenomenon is observed for the SCO configuration at 30.4 °C, since when extracting from the subcooler

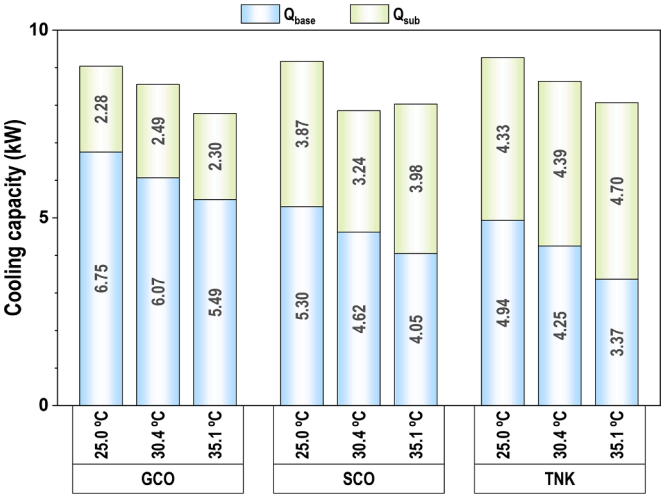

Fig. 12. Cooling capacity divided into subcooler capacity and base cycle capacity.

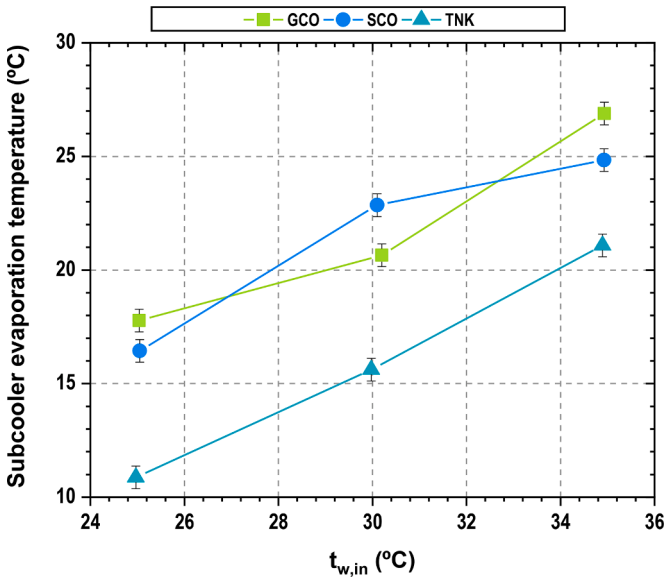

Fig. 13. Subcooler cooling capacity (left) and subcooler evaporation temperature (right).

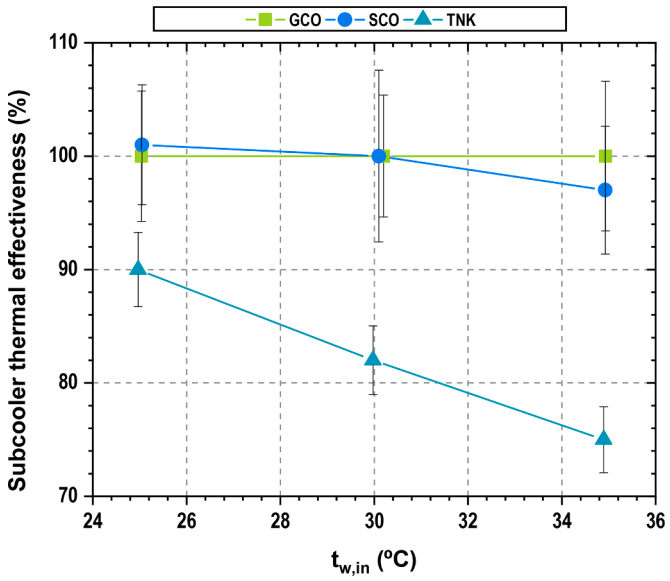

Fig. 14. Subcooler thermal effectiveness.

outlet, it is at this temperature where the system operates closer to the pseudocritical temperature.

From Fig. 10 it could be thought that it is not necessary to control the subcooling degree, but that each configuration has a different optimum does not mean that the control of this parameter is not important. In previous studies (Nebot-Andrés et al., 2020), the sensitivity of this parameter was analysed and it was concluded that the COP is more sensitive to gas-cooler pressure but that subcooling degree is also very important.

4.3. Behaviour of the subcooler

One of the most important components of the integrated mechanical subcooling cycle is the subcooler. In this work, where three possible architectures are analysed, the same heat exchanger is used for all three, thus being the same exchange surface in all cases. As seen in the previous section, although the optimal pressure conditions are the same for the three cycles, there are significant differences in the optimal subcooling degree. It is therefore necessary to analyse the behaviour of the subcooler for each of the cases.

Fig. 12 shows the cooling capacity of each of the configurations divided into the cooling capacity provided by the subcooler and the cooling capacity provided by the base cycle. The green bars show the subcooler cooling capacity for each of the optimum points, calculated as Eq. (1). The cooling capacity of the base cycle is the cooling capacity of the cycle if it was not subcooled, so calculated as stated in Eq.**Error! Reference source not found.**. As it can be clearly seen, each configuration requires different cooling capacity in the subcooler. The TNK configuration has the highest subcooler cooling capacity, being this fairly constant throughout the three test conditions. The SCO configuration exchanges lesser and the GCO configuration is the one with the least exchange. Specifically, the cooling capacity of the GCO configuration is 47% lower than the TNK.

$$\dot{Q}_{base} = \dot{Q}_0 - \dot{Q}_{sub} \tag{9}$$

As it can be seen, as the cooling capacity in the subcooler is higher for the TNK configuration and the overall cooling capacity is very similar for the three configurations, so the TNK has lower cooling capacity coming from the base cycle. Contrary, the 75% of the cooling power of the GCO configuration comes from the base cycle and the subcooler only represents around 25% of the contribution. A big difference between the configurations is seen. In the TNK configuration, the subcooler represents more than 50% of the cooling capacity, while in GCO it represents only 25%. This has a direct impact on the size of the heat exchanger.

Fig. 13 shows the evaporation temperature at the subcooler. As it can be seen, the three configurations follow an upward trend, the evaporation temperature being higher the higher the water temperature is. SCO and GCO have quite similar evaporation temperatures, between 1 and 2 K difference between them. It is the TNK configuration that presents the greatest differences, with an evaporation temperature between 5 and 6 K lower than the other two. This is due to the fact that this temperature will always be limited by the pressure of the tank (equivalent to the maximum evaporating temperature in the subcooler) in the TNK configuration, being therefore lower than the other two configurations that do not have this limitation.

Comparing SCO and GCO at 30.5 °C a slight difference in the evaporation temperature is also found. This is related to the subcooling degree. Thermal effectiveness of the subcooler is the practically the same for both configurations at this point but this is the point where maximum differences in the subcooling degree are obtained. The heat transfer in the subcooler depends both in the inlet and outlet temperatures of the subcooler (so on the subcooling degree) and the evaporation level on the subcooler. So, for 30.5 °C, if the temperatures at the exit of the subcooler are analysed, 20.1 °C are measured for GCO configuration and 21.7 °C for SCO, which is a difference of 1.6 K. Regarding the evaporation level, it is seen that the behaviour is coherent: for the GCO evaporation temperature is around 21 °C and for the SCO is around 23 °C, higher than for GCO.

Fig. 14 shows the thermal effectiveness of the subcooler (ε_{sub}) and its uncertainty. The thermal effectiveness is calculated as stated in Eq. **Error! Reference source not found.**. As can be seen in the figure, for GCO and SCO the efficiency is very high, because the cooling capacity is lower, and therefore the exchange area is better used. In many of the tests, the measured efficiency is near to 100% due to the measurement uncertainty of the thermocouples. It can be concluded that this efficiency will be high, although never equal to 100%. Regarding the TNK configuration, the efficiency of the subcooler is lower, decreasing when water temperature increases. This is because the evaporation temperature is lower and therefore the temperature pinch in the subcooler is higher than in the other configurations.

$$\varepsilon_{sub} = \frac{t_{gc,o} - t_{sub,o}}{t_{gc,o} - t_{0,sub}} = \frac{SUB}{t_{gc,o} - t_{0,sub}} \tag{10}$$

Table 1
IMS compressor's main parameters.

	$t_{w,in}$ (°C)	IMS compressor				
		η_{glo}	η_{vol}	τ	f_{IMS} (Hz)	t_{suc} (°C)
GCO	25.0	0.61	0.41	1.40	25	22.0
	30.2	0.73	0.49	1.46	30	24.9
	34.9	0.66	0.50	1.40	30	31.0
SCO	25.1	0.73	0.50	1.45	30	20.7
	30.1	0.68	0.41	1.36	25	27.3
	34.9	0.69	0.48	1.49	30	29.1
TNK	25.0	0.67	0.45	1.68	30	27.4
	30.0	0.81	0.45	1.65	30	33.1
	34.9	0.65	0.47	1.60	30	38.1

4.4. Behaviour of the IMS compressor

As mentioned in the previous sections, the IMS system bases its operation on the use of an auxiliary compressor that recompresses to gas-cooler pressure a part of the CO_2 mass flow that has been evaporated in the subcooler. The operation of this compressor is very particular since it must adapt its rotational speed to obtain a specific subcooling degree for which the plant's COP is maximum.

Table 1 sums up the main operating parameters of the IMS compressor for the optimal points that have been obtained experimentally and presented in the previous section. The presented parameters are the rotation frequency, the compression ratio, the overall and volumetric performances and the suction temperature. As can be seen in the table, the compression ratios of all the tests of configurations GCO and SCO are very low and specifically less than 1.5 for some test cases. These compression ratios are outside the operating range of the compressors, which should work over a compression ratio of 1.5. Regarding the frequency, we observe that all the optimal points are achieved with very low frequencies, in some cases lower than 30 Hz. For this type of plant, a smaller compressor should therefore be implemented, but the one used is the smallest existing of this type of compressors. Regarding the volumetric efficiency, the IMS compressor operates with values between 40 and 50% and the global efficiency's values are also quite low. Finally, another operating parameter that needs to be highlighted is the temperature obtained in the suction of the compressor, which, as can be seen in Table 1, is always higher than the compressor suction temperature limit, which is 10 °C.

In Fig. 15 the application limits of this particular compressor in terms of gas-cooler pressure and evaporation temperature can be seen (DORIN, 2018). The experimental data measured in the plant for the IMS compressor are shown in coloured points. As can be clearly seen, although the pressure levels are correct, the evaporation temperature of the IMS cycle is too high, falling outside the compressor operation boundary.

Although the IMS system is a very interesting system for its application in transcritical CO_2 cycles, at this time there is no CO_2 compressor specifically designed to work in the optimal system conditions, since they require very high suction temperatures, small sizes and low compression rates.

5. Conclusions

The experimental comparison of a CO_2 transcritical refrigeration plant working with integrated mechanical subcooling (IMS) with three different architectures is presented in this work. The difference between the configurations lies in the extraction point from which the expansion will take place in the IMS. The three possible extraction points are: the gas-cooler outlet (GCO), the subcooler outlet (SCO) or from the liquid tank (TNK). The comparison covered three heat rejection temperatures (25.0 °C, 30.4 °C and 35.1 °C) at steady-state conditions for optimum conditions where the COP is maximum for each configuration.

The results obtained show that there are no significant differences in the energetic behaviour of the three configurations, being that the COP of all of them is very similar for all conditions. Despite this, it is in the GCO configuration where higher COP values have been measured. Regarding the cooling capacity of the overall system, it is seen that it is the TNK configuration the one that presents the highest cooling capacity values. This is due to the fact that this is the configuration that presents higher values of optimal subcooling degree, a parameter directly related to the increments in the cooling capacity.

In this study it is observed that the main difference between the configurations resides in the subcooler. The optimal subcooling degree, the thermal effectiveness of the subcooler, its evaporation temperature and also the cooling capacity exchanged in this heat exchanger have been analysed in this work. It has been seen that all these parameters are

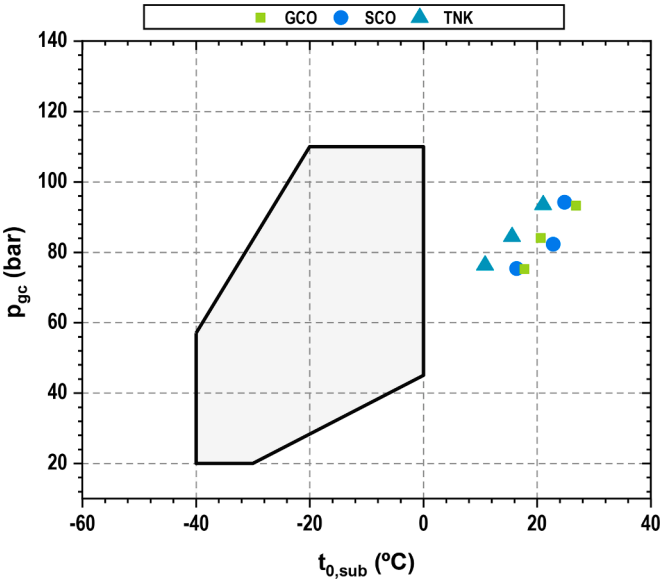

Fig. 15. Application limits of the IMS compressor and experimental points of operation.

Table 2
Main experimental results and uncertainty measurements of the optimum conditions.

	t_0 (°C)	$t_{w,in}$ (°C)	$p_{gc,o}$ (bar)	$t_{gc,o}$ (°C)	SUB (°C)	$\dot{m}_0$ (kg/s)	$P_{c,main}$ (kW)	$P_{c,IMS}$ (kW)	$\dot{Q}_0$ (kW)	$\varepsilon(\dot{Q}_0)$ (%)	COP (-)	ε(COP) (%)
GCO	-9.1	25.0	76.1	30.2	12.7	0.04	3.60	0.61	9.04	0.87	2.15	0.98
	-8.8	30.2	85.1	34.1	14.0	0.04	3.89	0.74	8.56	0.89	1.85	0.98
	-7.9	34.9	94.1	38.1	12.2	0.04	4.16	0.77	7.78	1.02	1.58	1.10
SCO	-9.2	25.0	76.2	30.2	14.3	0.04	3.60	0.67	9.17	0.83	2.15	0.93
	-10.3	30.1	83.2	33.1	11.4	0.04	3.78	0.63	7.85	0.95	1.78	1.04
	-7.7	34.9	95.2	37.4	13.4	0.04	4.24	0.83	8.03	0.95	1.58	1.05
TNK	-9.5	25.0	77.1	29.5	16.9	0.04	3.56	0.77	9.27	0.77	2.14	0.88
	-9.0	30.0	85.1	33.4	14.9	0.04	3.88	0.82	8.64	0.84	1.84	0.94
	-7.5	34.9	94.1	37.7	13.0	0.04	4.20	0.88	8.07	1.00	1.59	1.09

different for each of the configurations. From the analysis of these parameters, it can be concluded that the SCO and GCO configurations need a smaller subcooler since they present greater thermal effectiveness and the heat they must exchange is also much lower. This also implies a lower cost when assembling said cycle.

From this experimental work it can be concluded that the IMS cycle is a very versatile system for the improvement of transcritical CO_2 cycles since it can be designed in three different ways without having noticeable losses in its energetic performance. However, there is room for improvement since, the auxiliary compressor works outside its operability range. Therefore, the design of compressors adapted to this application would be interesting. The best configuration is the extraction from the gas-cooler outlet since the three configurations present similar energetic behaviour but it requires much lower cooling capacity in the subcooler.

Author contributions statements

L.N. developed the idea, performed the tests and wrote the manuscript. D.C. and C.F. helped to perform the tests. R. Ll. supervised the work and made final proofreading. D.S. and R.C. helped to get funds.

Declaration of Competing Interest

The authors declare that they have no known competing financial interests or personal relationships that could have appeared to influence the work reported in this paper.

Acknowledgements

The authors thank the Ministerio de Ciencia y Tecnología (Spain) project RTI2018–093501-B-C21, the Ministerio de Educación, Cultura y Deporte (Spain), grant FPU16/00151 and the Jaume I University (Spain), project UJI-B2019–56 and grant PREDOC/2019/19 for financing this research work.

References

Catalán-Gil, J., Llopis, R., Sánchez, D., Nebot-Andrés, L., Cabello, R., 2019. Energy analysis of dedicated and integrated mechanical subcooled CO 2 boosters for supermarket applications. Int. J. Refrig. 101, 11–23.

Cortella, G., Coppola, M.A., D'Agaro, P., 2021. Sizing and control rules of dedicated mechanical subcooler in transcritical CO2 booster systems for commercial refrigeration. Appl. Therm. Eng. 193.

DORIN, 2018. CO2 semi-hermetic compressors, cd series. CO2 Transcritical Application. Officine Mario Dorin S.p.A., Italy.

European Commission, 2014. Regulation (EU) No 517/2014 of the European Parliament and of the Council of 16 April 2014 on fluorinated greenhouse gases and repealing Regulation (EC) No 842/2006.

Gullo, P., Hafner, A., Banasiak, K., 2018. Transcritical R744 refrigeration systems for supermarket applications: current status and future perspectives. Int. J. Refrig. 93, 269–310.

Gullo, P., Hafner, A., Banasiak, K., Minetto, S., Kriezi, E.E., 2019. Multi-ejector concept: a comprehensive review on its latest technological developments. Energies 12.

Karampour, M., Sawalha, S., 2018. State-of-the-art integrated CO2 refrigeration system for supermarkets: a comparative analysis. Int. J. Refrig. 86, 239–257.

Lawrence, N., Elbel, S., 2019. Experimental investigation on control methods and strategies for off-design operation of the transcritical R744 two-phase ejector cycle. Int. J. Refrigeration 106, 570–582.

Lemmon, E.W., Huber, M.L., McLinden, M.O., 2013. REFPROP, NIST Standard Reference Database 23, v.9.1. National Institute of Standards, Gaithersburg, MD, U.S.A.

Liao, S.M., Zhao, T.S., 2002. Measurements of heat transfer coefficients from supercritical carbon dioxide flowing in horizontal mini/micro channels. J. Heat Transf. 124, 413–420.

Llopis, R., Cabello, R., Sánchez, D., Torrella, E., 2015. Energy improvements of CO2 transcritical refrigeration cycles using dedicated mechanical subcooling. Int. J. Refrig. 55, 129–141.

Llopis, R., Nebot-Andrés, L., Cabello, R., Sánchez, D., Catalán-Gil, J., 2016. Experimental evaluation of a CO2 transcritical refrigeration plant with dedicated mechanical subcooling. Int. J. Refrig. 69, 361–368.

Llopis, R., Nebot-Andrés, L., Sánchez, D., Catalán-Gil, J., Cabello, R., 2018. Subcooling methods for CO2 refrigeration cycles: a review. Int. J. Refrig. 93, 85–107.

Moffat, R.J., 1985. Using uncertainty analysis in the planning of an experiment. J. Fluids Eng. 107, 173–178.

Nebot-Andrés, L., Calleja-Anta, D., Sánchez, D., Cabello, R., Llopis, R., 2019. Thermodynamic analysis of a CO2 refrigeration cycle with integrated mechanical subcooling. Energies 13.

Nebot-Andrés, L., Catalán-Gil, J., Sánchez, D., Calleja-Anta, D., Cabello, R., Llopis, R., 2020. Experimental determination of the optimum working conditions of a transcritical CO2 refrigeration plant with integrated mechanical subcooling. Int. J. Refrig. 113, 266–275.

Nebot-Andrés, L., Sánchez, D., Calleja-Anta, D., Cabello, R., Llopis, R., 2021a. Experimental determination of the optimum intermediate and gas-cooler pressures of a commercial transcritical CO2 refrigeration plant with parallel compression. Appl. Therm. Eng. 189.

Nebot-Andrés, L., Sánchez, D., Calleja-Anta, D., Cabello, R., Llopis, R., 2021b. Experimental determination of the optimum working conditions of a commercial transcritical CO2 refrigeration plant with a R-152a dedicated mechanical subcooling. Int. J. Refrig. 121, 258–268.

Rigola, J., Ablanque, N., Pérez-Segarra, C.D., Oliva, A., 2010. Numerical simulation and experimental validation of internal heat exchanger influence on CO2 trans-critical cycle performance. Int. J. Refrig. 33, 664–674.

Sarkar, J., Agrawal, N., 2010. Performance optimization of transcritical CO2 cycle with parallel compression economization. Int. J. Thermal Sci. 49, 838–843.